Multiparameter analysis of vascular remodeling in post-acute sequelae of COVID-19

Mathilde Maury, Aurélien Justet, Juliette Dindart, Jean Richeux, Lucile Sese, Nicolas Aide, Thomas Gille, Hilario Nunes, Jean-François Bernaudin, Pierre-Yves Brillet, et al.

Multiparameter analysis of vascular remodeling in post-acute sequelae of COVID-19

Catalin Fetita[1], Mathilde Maury[1], Aurélien Justet[2], Juliette Dindart[3], Jean Richeux[2], Lucile Sese[3,4], Nicolas Aide[2], Thomas Gille[3,4], Hilario Nunes[3,4] Jean-François Bernaudin [3,4,5,] and Pierre-Yves Brillet[3,4]

[1]SAMOVAR, Telecom Sud-Paris, Institut Polytechnique de Paris, Evry, France
[2]Pneumologie & Médecine Nucléaire CHU Caen, France
[3]Avicenne Hospital, AP-HP, Bobigny, France
[4]INSERM 1272 Université Sorbonne Paris Nord, Bobigny, France
[5]Sorbonne Université Paris

Abstract. The COVID-19 infection, a current worldwide health concern, manifests as an alveolar-interstitial pneumonia with unknown long-term evolution. It is also associated with vascular dysfunction and shows a vascular remodeling with a changed balance between small- and large-caliber vessels. In this study, we question the existence of residual vascular alteration in post-acute sequelae of COVID-19 (PASC) by investigating possible associations between vascular remodeling biomarkers extracted from CT and functional, radiological and morphological parameters. The used vascular biomarkers concern the blood volume ratio of vessels with cross-section area inferior to 5 mm^2 versus vessels of cross-section area inferior to 50 mm^2 (BV5/BV50), an index of local peripheral vascular density and a peripheral composite vascular remodeling index, both measured in the antero-postero-lateral lung periphery (excluding mediastinal region). As a functional parameter, diffusing capacity of the lung for carbon monoxide (DLCO) is a measure depending on the vascular perfusion and the amount of interstitial thickening, a decreased DLCO value suggesting altered vascular perfusion. Imaging biomarkers can be extracted from the analysis of perfusion lung scintigraphy or CT scan. Some of them are included in our study. Radiological features include CT attenuation as a measure of persistence of ground glass opacity and development of changes suggestive to look for fibrosis, such as reticulations. As additional morphological parameter, lung deformation observed between inspiration/expiration maneuvers may be suggestive of the presence of reticulations inducing lung stiffness and breathing deficiency.
The investigation of associations between vascular remodeling biomarkers obtained from CT and the above functional, radiological and morphological parameters revealed moderate to strong correlations highlighting the ability to capture the persistence of vascular alterations in PASC in relation with the development of fibrotic patterns, which is a promising direction for future research.

Keywords: post-acute sequelae of COVID-19 (PASC), vascular remodeling, lung deformation, peripheral vascular density, peripheral composite remodeling index, lung perfusion scintigraphy, computed tomography

1. Description of purpose

COVID-19 infection, a recent worldwide health concern, presents several similarities with fibrosing interstitial pneumonia (fIIP) involving the vascular and alveolar-interstitial pulmonary compartments with an unknown long-term evolution. There are assumptions that this condition is likely to evolve to fIIP in 10-30% of severe cases [1]. However, the main differences between COVID-19 and fIIP are the preponderance of peripheral ground glass opacities, as well as, to the best of our knowledge, the absence of non-reversible airway remodeling.
COVID-19 is also known to induce an acute vascular dysfunction with a vascular remodeling changing the balance between small- and large-caliber vessels. In two recent works, Synn et al [2] and Lins et al [3] showed that the blood volume ratio of vessels with cross-sectional area < 5 mm^2 (denoted by BV5) versus total blood volume (TBV), respectively versus vessels of cross-sectional area smaller than 10 mm^2 (BV10), was a robust biomarker of vessel pruning. Lower values of BV5/TBV or BV5/BV10 indicate higher pruning, which was proven to correlate with the mortality rate [2] and with the COVID condition [3].

In this study we question the existence of residual vascular alteration in post-acute sequelae of COVID-19 (PASC) by

investigating possible associations between vascular biomarkers extracted from CT and functional, radiological and morphological parameters. The used vascular biomarkers concern the blood volume ratio of vessels with cross-section area inferior to 5 mm^2 versus vessels of cross-section area inferior to 50 mm^2 (BV5/BV50), an index of local peripheral vascular density and a peripheral composite vascular remodeling index, both measured in the antero-postero-lateral lung periphery (excluding mediastinal region). Diffusing capacity of the lung for carbon monoxide (DLCO) is a measure depending on the vascular perfusion and the interstitial remodeling expressed as reticulations, therefore a decreased DLCO value suggests altered vascular perfusion. Additional clinical biomarkers may result from perfusion scintigraphy and some of them are included in our study. Radiological parameters include CT attenuation as a measure of persistence of ground glass opacity and development of changes suggestive of fibrosis, such as reticulations. In addition, lung deformation observed between inspiration/expiration maneuvers may highlight the presence of reticulations inducing lung stiffness and breathing deficiency.

2. Materials and methods

Two CT datasets were collected from different on-going studies on COVID-19:

1. A 10-patient follow up dataset collected at Caen University Hospital, France.
All patients included performed lung function test, CT inspiratory and expiratory scans and lung perfusion scintigraphy, 6 months after a severe COVID episode.

2. A follow-up dataset selected from the *Silicovilung* project cohort of Avicenne Hospital - APHP, Bobigny, France, gathering patients with strict inclusion criteria:

- severe COVID initial episode without mechanical ventilation
- absence of underlying pulmonary interstitial disease,
- presence of inspiratory CT at inclusion (M0),
- CT inspiratory and expiratory scans and functional respiratory tests after three months (M3)
- follow-up examination planned after 12 months (M12)

At the time of our study, 27 patients were selected from 58 eligible subjects of the *Silicovilung* cohort, for which only CT data at M0 and M3 were fully available.

From the CT data available in these cohorts, several vascular and morphological biomarkers potentially revelatory of COVID-19 phenotype were extracted and analyzed as follows. Note that for inter-patient comparison purposes, all CT datasets were resampled isotropically at 0.6 mm per pixel in the x-,y-,z- direction.

2.1 Scintigraphy biomarkers

In ten patients, both CT scan and lung perfusion scintigraphy allowed to investigate possible correlation between results obtained from these different tools, performed 6 months after acute COVID. Note that, the interpretation of perfusion defects in scintigraphy is rather qualitative and relies on the visual assessment of the heterogeneity of the peripheral zones in the perfusion maps. In order to translate such qualitative assessment into a quantitative biomarker, the antero-postero-lateral lung periphery of the volumetric lung perfusion maps was “unfolded” on a 2D image using a radial projection of each lung. The lung segmentation from the perfusion masks was obtained by simple thresholding, 3D-connected component analysis and 3D morphological closing. The lung periphery was defined outside of the mediastinal zone in a bandwidth either selected as a percent (20%) of the maximal lung diameter (measured on axial images) or as a fixed value (2 cm). Subsequent experiments showed that the second choice avoids large variability between subjects, and was the option finally chosen. (Fig. 1a). The apical-to-basal projection of each segmented lung allows computing the lung orientation using principal component analysis of the generated shape. In this way, the radial projection designed to “unfold” the peripheral lung region (Fig. 1b) is always oriented in the sagittal lung direction irrespective to the lung rotation. The radial projection involves an aperture of 180° with 0.5° between each projection ray and is performed on each axial slice of the perfusion volume. The generated peripheral perfusion maps (Fig. 1c) exploit a composite value integration along each projection ray, inside the peripheral areas.

A global image biomarker is computed from each peripheral perfusion map as the average value of the map. Such biomarker is referred to as ***peripheral perfusion scintigraphy index*** (**SPI**). Note that more complex measures can be used

here, but they were not considered in this study. The SPI biomarker will be compared in the experimental section with the DLCO measures in the same patients, to investigate potential relationship between these parameters.

An interesting question was to explore the relationship between the SPI functional parameter extracted from scintigraphy data and morphological biomarkers computed from the analysis of the vascular geometry and shape, extracted from the CT data acquired in the same subjects. The different CT vascular biomarkers proposed are presented in section 2.2.

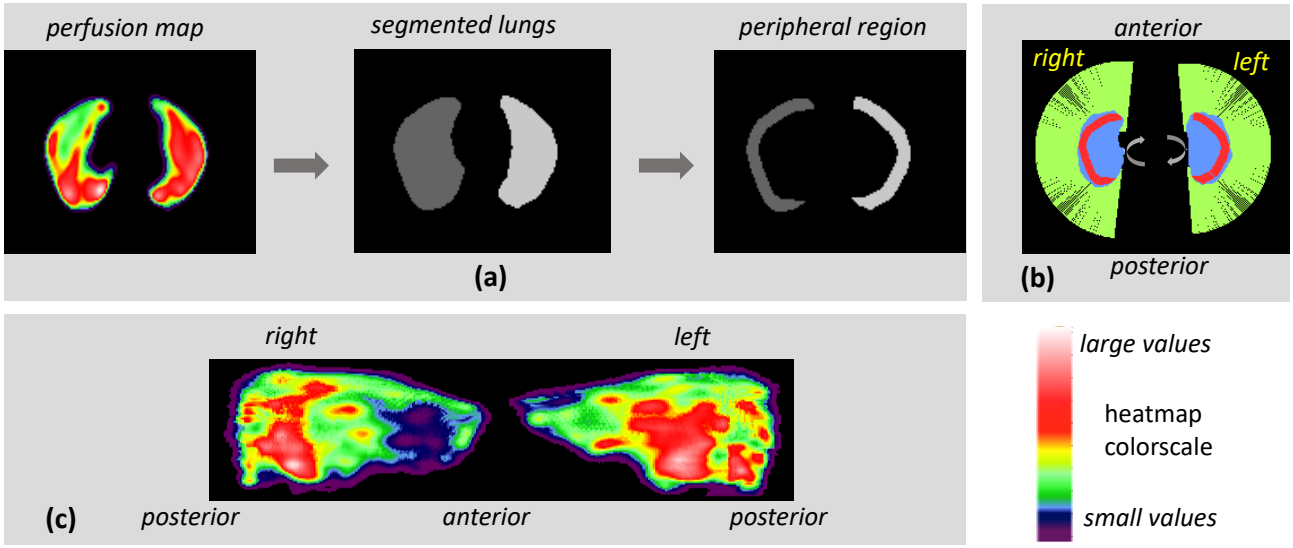

Fig.1. Generation of the peripheral "unfolded" perfusion maps: (a) lung segmentation from perfusion maps (heatmap color) and definition of the peripheral lung region; (b) radial projection scheme of the peripheral region (red) of each lung: in blue, apical-basal projection of the lung used to compute the sagittal lung orientation; (c) peripheral perfusion maps shown as heatmap colors (warmer color denotes larger value).

2.2 CT vascular biomarkers

The intrapulmonary vascular structures were automatically segmented by exploiting the approach in [4], which is robust with respect to the pathology presence, e.g. ground glass and fibrotic reticulations; in regions with high reticulation density where vessels cannot be discriminated, the algorithm prevents for false-positive extraction. An additional vessel propagation step from terminal segments was developed in order to capture a maximum of smallest caliber vessels; this step allows achieving comparable vascular segmentation performance for CT datasets with different levels of contrast.

The vessel propagation procedure was inspired from the approach for distal airway segmentation developed in [5], by taking as input data the negative grayscale volume of the thorax, where vessels will have features similar with airway lumen on original CT data.

After segmentation, the local radius in each point of the vessel tree is computed by means of a morphological granulometry using a spherical structuring element [7]. Figure 2 shows an example of segmented pulmonary vascular tree, before and after using the additional distal propagation procedure.

A first global biomarker, computed based on caliber information, was the blood volume ratio BV5/BV50 as an indicator of vessel caliber remodeling, where decreased values correspond to a shift of caliber distribution to larger diameters (pruning of small-caliber vessels and/or vasodilation).

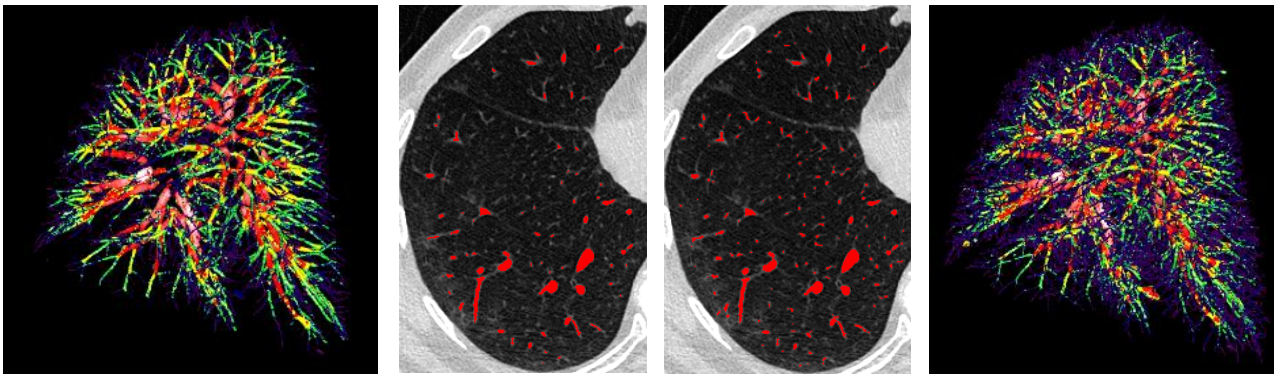

3D rendering of vascular calibers *axial view* *axial view* *3D rendering of vascular calibers*

(a) initial segmentation using the approach in [4] (b) final segmentation after the new propagation step

Fig. 2. 3D rendering of vascular tree with calibers displayed as false colors (heatmap) and same axial slice comparison with segmented vessels superimposed in red: the final segmentation shows small-caliber vessels recovery.

In addition, three 3D local vascular maps were generated as potential competitors to the scintigraphy perfusion maps (Fig. 3). Each map integrates in one voxel a specific measure achieved on the vessel tree in a corresponding region of interest ROI=2x2x2 cm^3. The ROI is shifted on the vascular volume with a stride of 2, leading to vascular maps of half-coarser spatial resolution (and half size). The three measures considered in the ROI are as follows:

(1) the ***local vascular density of small-to-medium caliber vessels (LVD)*** estimated in the 2x2x2 cm^3 ROI (Fig. 3b):

$$LVD = BV20/V_{ROI}\,, \tag{1}$$

where BV20 denotes the volume of blood vessels of cross-section area smaller than 20 mm^2 (radius < 2.5 mm) and V_{ROI} the volume of the ROI where BV20 is evaluated (i.e. 8 cm^3),

(2) the ***local BV5/BV50 ratio (LBV5-50)*** in the ROI, Fig. 3c, and

(3) the ***composite vascular remodeling index (CVI)***, measured as local vascular density multiplied by the local BV5/BV50 ratio LBV5-50 (Fig. 3d):

$$CVI = LVD \cdot LBV5\text{-}50. \tag{2}$$

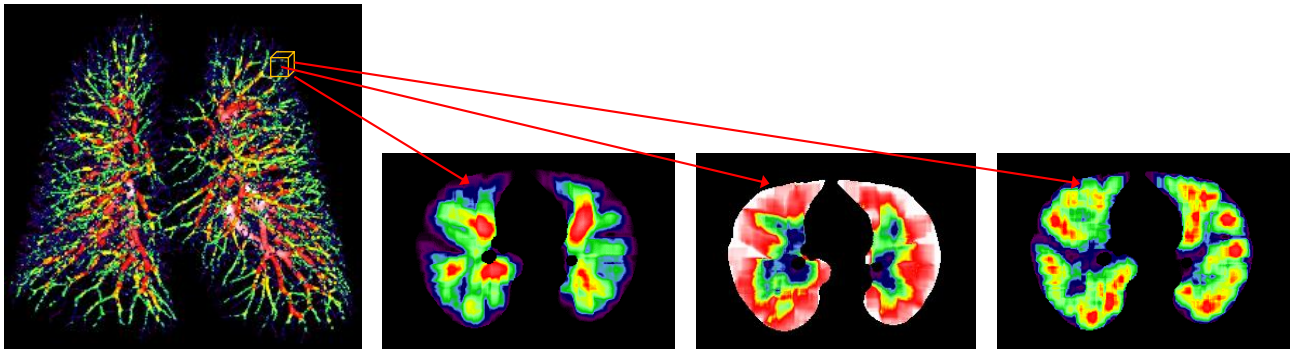

(a) (b) LVD (c) LBV5-50 (d) CVI

Fig. 3. Computation of local vascular maps based on the 3D vascular calibers using a sliding bounding box (a); example of axial cross-sections (heatmap color coding) of local vascular density map, LVD (b), local BV/BV50 ratio, LBV5-50 (c), and composite remodeling map, CVI (d).

Note that the LVD map informs on the local ROI volume percent occupancy by vessels of radius < 2.5 mm at each point in the lung. Lung peripheral regions in the map show thus smaller values since this area contains only small caliber vessels which segmentation is limited by the image spatial resolution and contrast. The LBV5-50 map shows instead high values at lung periphery since the ratio BV5/BV50 (i.e. volume ratio of vessels of radii < 1.26 mm versus vessels of radii < 4 mm) is high due to the absence of larger caliber vessels in this area. The CVI map tries to achieve a trade-off between vascular occupancy and the absence of small vessel pruning in order to focus on the distribution of small vessels in the lung. CVI penalizes local vascular density (LVD) values in areas sparsely populated with small-caliber vessels and keeps them unchanged at sites where large-caliber vessels are rare.

For the sake of comparison with scintigraphy-based measurements, we need to generate the same peripheral maps related to the LVD, LBV5-50 and CVI maps in the antero-latero-posterior lung peripheral area, using the same procedure as in section 2.1. For this purpose, the lung segmentation from CT data is obtained based on the approach in [6] and the same peripheral bandwidth of 2 cm is considered for peripheral lung "unfolding". Fig. 4 illustrates these three peripheral maps together with a projection of vessel caliber distribution in the same area (using the same radial "unfolding" approach).

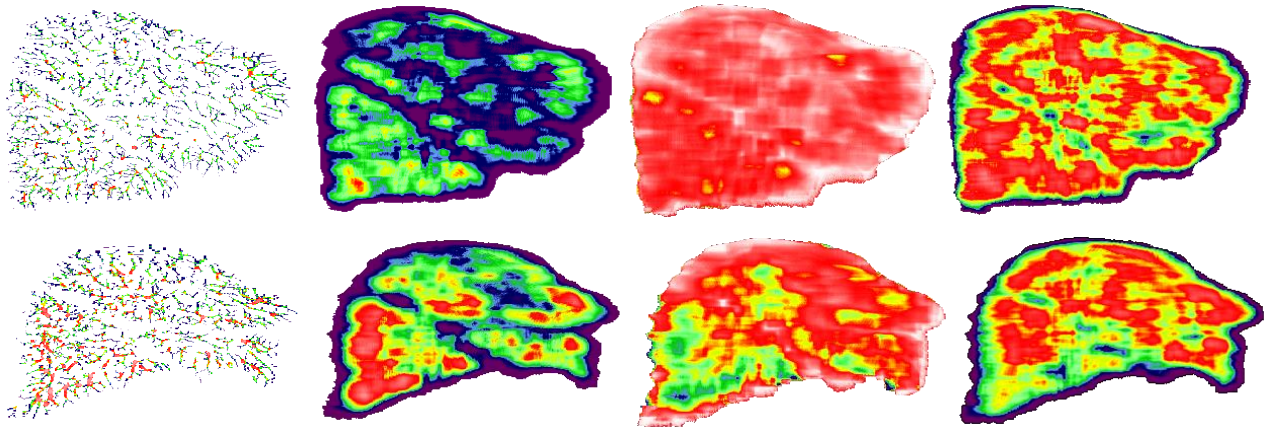

(a) PU-vascular calibers (b) PU-LVD (c) PU-LBV5-50 (d) PU-CVI

Fig. 4. Example of peripheral "unfolded" (PU-) maps (right lung) for two COVID-19 subjects with good (top) and altered (bottom) vascular perfusion (heatmap color). For visualization purposes, the resulting value range in these maps is extended to [0-255] by multiplication with different constant coefficient values, experimentally found (2000 in (b), 255 in (c) and 7700 in (d)). Top row subject the same as in Fig. 1.

In the example shown in Fig. 4, top row, we notice that in the vascular map Fig. 4a, the major part of vessels have small calibers all over the lung. The vascular density map PU-LVD, Fig. 4b, shows almost constant values induced by a similar amount of ROI occupancy of these small caliber vessels (exception being made for lung fissure regions with sparser vessel occurrence). Because of massive absence of larger-caliber vessels in this peripheral zone, the peripheral "unfolded" PU-LBV5-50 map (Fig. 4c) is also relatively uniform with values close to 1 and consequently the composite map PU-CVI will almost not modify the PU-LVD map (Fig. 4d). Conversely, for the bottom-row subject, higher vascular calibers are visible in the inferior right lobe, leading to higher vascular density PU-LVD and thus to smaller LBV5-50 values in this region which will modify the PU-CVI map.

As for the scintigraphy analysis, section 2.1, based on the "unfolded" peripheral maps (Fig. 4), three biomarkers are extracted as the average value of each map:

- an ***index of the peripheral vascular density***, **PVD**,

$$PVD = E(\text{PU-LVD}), \quad (3)$$

- a local BV5/BV50 index, **LBVI**,

$$LBVI = E(\text{PU-LBV5-50}), \text{ and} \quad (4)$$

- a ***peripheral composite remodeling index,*** **PCI**,

$$PCI = E(\text{PU-CVI}), \quad (5)$$

where E(.) denotes the expectation operator.

2.3. CT attenuation and lung deformation markers

The follow-up CT dataset allowed the definition and investigation of two additional biomarkers:
(1) the CT attenuation change between M0 and M3 scans for each lung based on sagittal projections (resp. Sag(M0) and Sag(M3)) obtained for the same orientations as in Fig. 1b but using parallel instead of radial projections (Fig. 5). As stated before and illustrated in Fig. 5, this ensures that the projection direction is preserved from one acquisition to another irrespective to patient rotations on the CT scan bed (the longitudinal orientation is considered the same, as being globally imposed by the scan bed geometry).

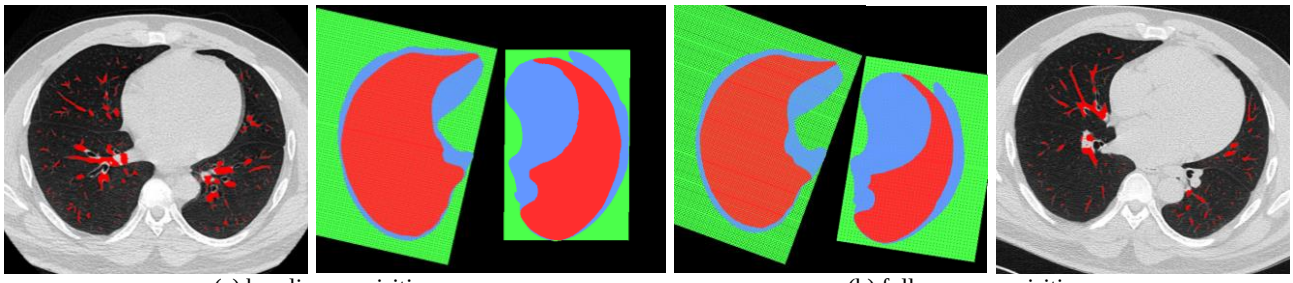

(a) baseline acquisition (b) follow-up acquisition

Fig. 5. Sagittal parallel projection scheme based on the estimation of lung orientation: red – segmented lung section, blue – apical-basal projection of the segmented lung (used for lung orientation estimation), green – projection rays.

As shown on the parallel sagittal projections of Fig. 6, in case of lung texture improvement (recovery of ground glass/infectious regions) at M3 vs M0, the difference between the average density at M3 and that at M0 measured on the registered image M0 to M3 will be negative with absolute value higher in case of improvement. A new marker will be defined based on this difference and referred to as ***CT attenuation improvement at M3,*** **CT_impM3**:

$$CT\_impM3 = E(\ Sag(M0_{reg(M3)})\ ) - E(M3), \quad (6)$$

where E(.) denotes the expectation operator, Sag(X) the sagittal projection of X lung and $M0_{reg(M3)}$ the registered image M0 to M3. CT_impM3 will be thus positive in case of CT density improvement at M3 versus M0.

(2) based on inspiration and expiration scans at M3, the average basal deformation of the lungs near the diaphragmatic region can be estimated from the same lung sagittal images (Fig. 7). This average deformation is normalized with respect to the height of the lung bounding box and the resulting biomarker is referred to as ***percent lung basal deformation at M3*** **(LBD)**. The 2D registration/interpolation approach used in this case is [8].

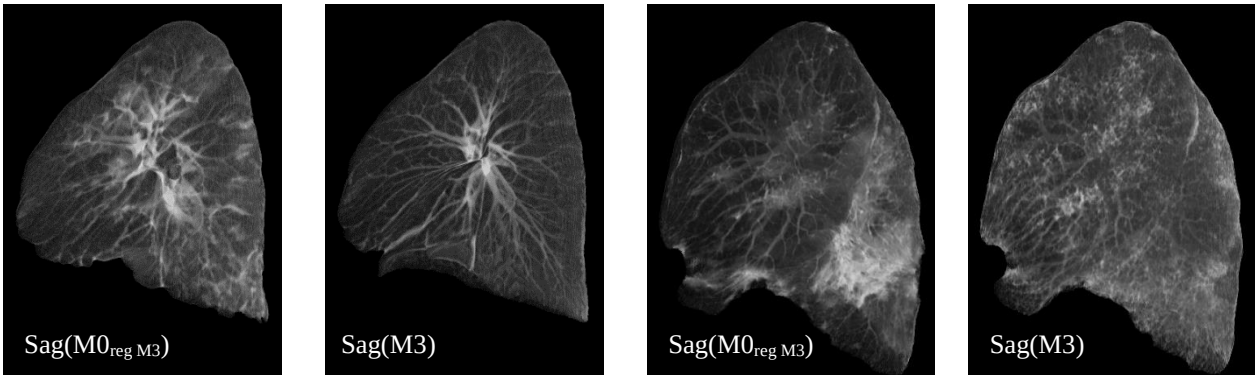

(a) state improvement (ground glass regions disappear at M3) (b) worsening (persistence/extension of fibrotic regions at M3)

Fig. 6. CT attenuation change between M0 (registered to M3) and M3, estimated on sagittal projections (here left lung shown).

The proposed vascular biomarkers were computed on both datasets (when appropriate) and possible associations between them and with functional data were investigated. The inclusion of subjects from the *Silicovilung* cohort in the correlation study was restricted to cases for which all biomarkers above could be obtained (valid segmentation of lungs and vessels at baseline and follow-up for both inspiration/expiration). The next session presents the experimental results obtained.

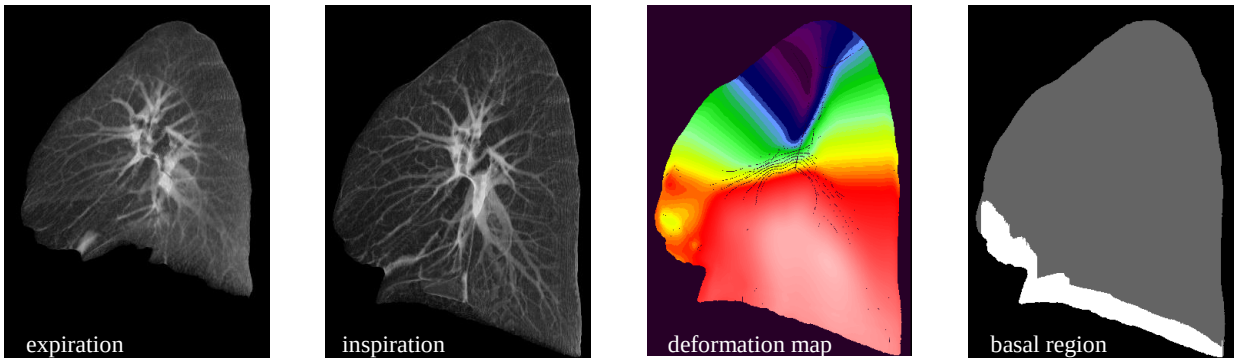

(a) (b)

Fig. 7. Estimation of the lung deformation in the basal region from the sagittal projection images at inspiration/expiration (a) at M3; (b) deformation map (local amplitude shown as heatmap color) and basal region (white) for average basal deformation estimation.

3. Results and discussion

3.1. Association between perfusion scintigraphy and computed tomography markers

The first attention was directed towards the analysis of peripheral vascular markers computed from CT data (PCI, PVD, LBVI) versus the peripheral marker derived from scintigraphy (SPI). The correlation matrices shown in Fig. 8 show high and significant correlation coefficients between PCI/PVD and SPI (mean value computed for both lungs). Weak or no correlation was found between the peripheral local BV5/BV50 index, LBVI and the other markers; this was more or less expected since in the lung periphery, medium-large caliber vessels are generally not present and thus the local BV5/BV50 ratio is generally high (close to 1). The LBVI decrease may be caused by small-caliber vessel remodeling in the lung periphery leading to a caliber increase of peripheral vessels over 1.26 mm radius, which probably does not occur for small perfusion defects that can be captured by scintigraphy (this hypothesis is also supported by the comparison between Fig. 4c top vs. Fig. 1). Of course, these findings have to be validated on an increased dataset of coupled acquisitions with CT and scintigraphy, which is planned in a future project. Nevertheless, the significant correlations found between peripheral markers PCI, PVD in CT and SPI in scintigraphy, validate the pertinence of these CT biomarkers and may suggest their potential as a surrogate for perfusion scintigraphy (which remains a costly and complex procedure) in COVID follow-up.

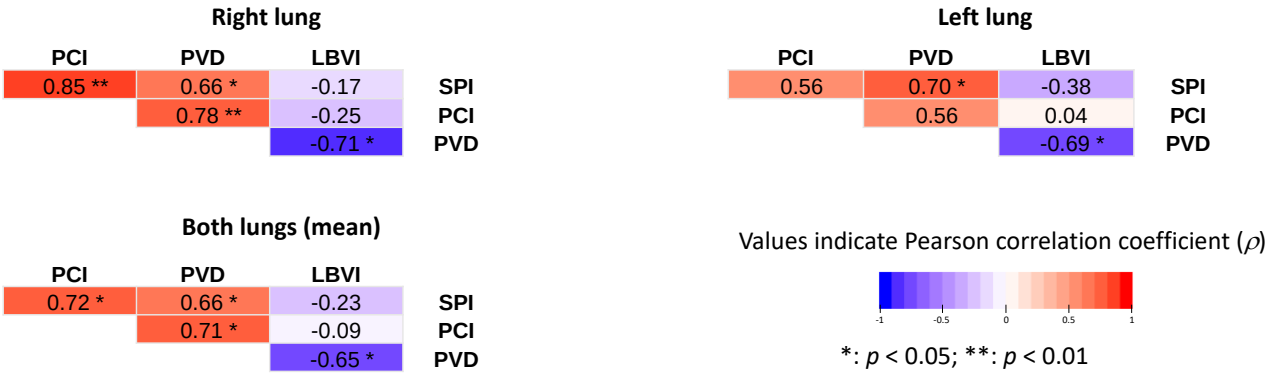

Fig. 8. Correlation between peripheral markers computed from CT and scintigraphy data (Caen cohort, 10 subjects).

Interestingly, the global vascular volume ratio BV5/BV50 did not correlate significantly to any of the peripheral markers computed on the first cohort (10 patients). A moderate correlation (almost significant) was however noticed with PCI score), Tab. 1a. A re-evaluation of BV5/BV50 association with the PCI and PVD scores on an extended cohort including 18 additional subjects from the *Silicovilung* database shows that the correlation between the global score BV5/BV50 and peripheral composite score PCI becomes significant, Tab. 1b. This suggests that PCI could be a key biomarker linking CT and scintigraphy and also peripheral vs global vascular remodeling.

Tab. 1. Association between global and peripheral vascular remodeling scores (Pearson correlation coefficient).

10 subjects	**SPI**	**PCI**	**PVD**	**LBVI**
BV5/BV50	0.104	0.56	0.23	0.17
p-value	*0.774*	*0.09*	*0.519*	*0.637*

(a) Caen cohort

28 subjects	**PCI**	**PVD**
BV5/BV50	**0.596**	0.07
p-value	*0.001*	*0.74*

(b) Caen + Silicovilung cohorts

3.2 Association between vascular markers and functional parameters

We investigate possible correlations between functional parameters (DLCO) and peripheral markers computed from perfusion scintigraphy and CT scans (on Caen cohort dataset). As shown in Fig. 9, moderate but not significant correlations were found with SPI, PCI and LBVI.

Fig. 9. Association between DLCO and peripheral markers from perfusion scintigraphy and CT (Caen cohort) expressed in terms of Pearson correlation coefficient.

When extending the dataset to *Silicovilung* cohort, a significant moderate-to-strong negative correlation was found between DLCO and peripheral vascular density, Tab. 2a. Interestingly, if we split the dataset according to the functional severity threshold of DLCO (DLCO </>70), strong significant negative correlations appear between the DLCO and both PCI and PVD, Tab. 2b. This may suggest an increased peripheral vascular remodeling for more altered alveolar-capillary diffusion (gas exchange), which might reflect both an increase in peripheral vascular density and higher occurrence of small caliber vessels. Two physiological questions arise: is this a phenomenon that participates in physiological healing with, if not neoangiogenesis, at least an increase in flow to areas that need it? Or is it that distal alveolar and/or vascular destruction will rarefy the capillary bed and cause "stasis" upstream? Figure 10 graphically illustrates the significant correlations of Tab. 2.

Tab. 2. Association between DLCO and CT biomarkers (Pearson correlation coefficient).

Caen + Silicovilung	**PCI**	**PVD**	**BV5/BV50**
DLCO	-0.195	**-0.608**	0.114
p-value	*0.319*	*0.0006*	*0.561*

(a) overall analysis

Caen + Silicovilung	**PCI**	**PVD**	**BV5/BV50**
DLCO < 70	**-0.77**	**-0.758**	-0.469
p-value	*0.002*	*0.002*	*0.105*
DLCO >= 70	0.306	0.155	-0.0077
p-value	*0.267*	*0.58*	*0.978*

(b) analysis based on functional severity

3.3 Association between vascular markers computed on follow-up data

As shown in section 3.1, a moderate significant correlation between BV5/BV50 ratio and peripheral composite index PCI was found for CT image data acquired 3 months after inclusion, Tab. 1b. When investigating the relationship between the variation of the same markers between baseline and 3-months follow-up (*Silicovilung* cohort), we found a similar significant moderate correlation ($\rho = 0.54$, $p=0.03$), Fig. 11a.

It is worth mentioning that a moderate correlation, almost significant, was noticed between peripheral vascular density PVD at baseline (M0) and CT attenuation improvement at M3 ($\rho = 0.48$, $p=0.07$). If this trend is confirmed on further patient inclusions, PVD at baseline could be seen as a predictive marker of evolution of lung opacification at follow-up.

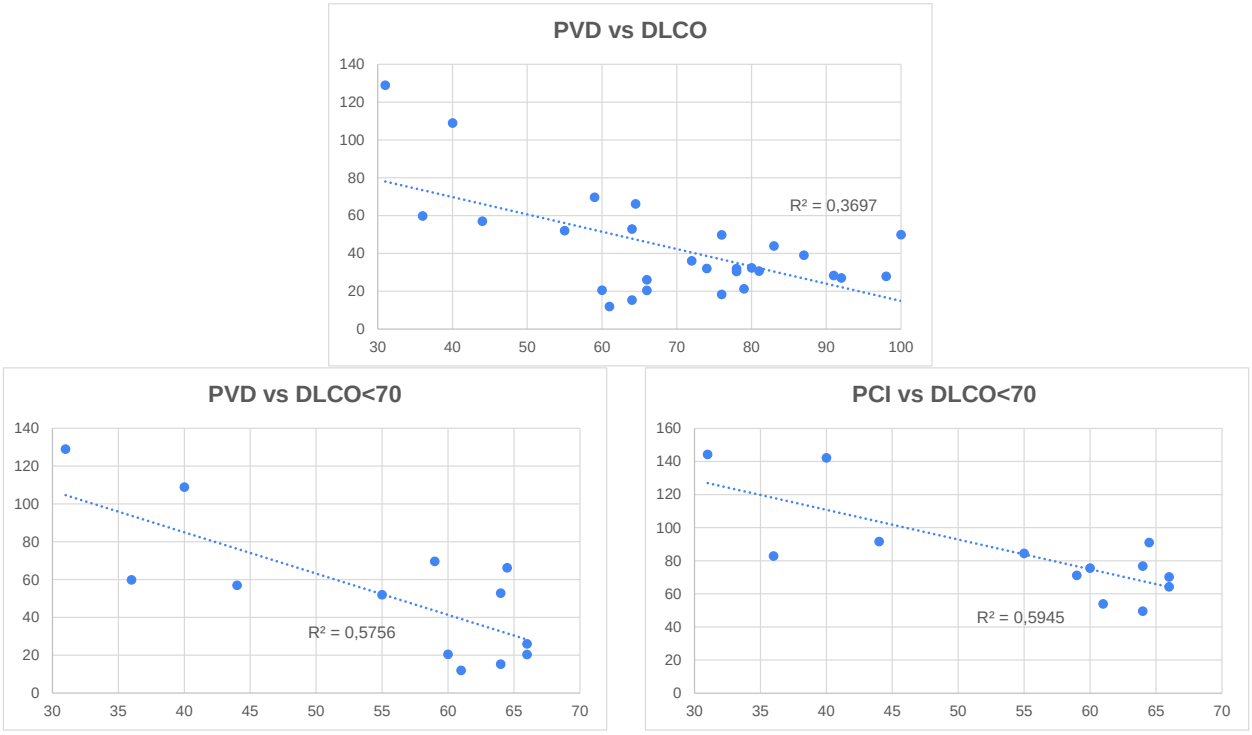

Fig. 10. Illustration of significant associations found in Tab. 2.

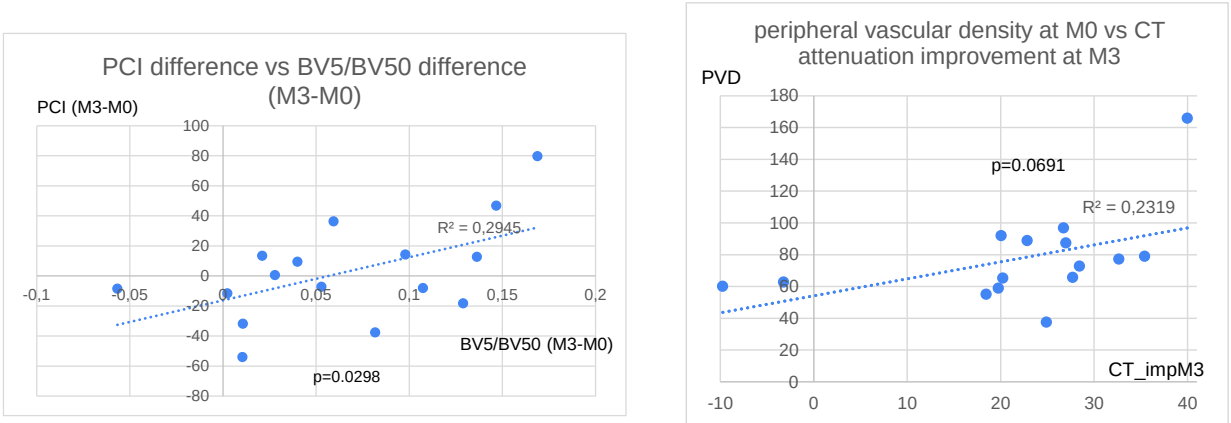

(a) peripheral vs global vascular remodeling markers

(b) vascular markers vs lung opacification

Fig. 11. Associations between vascular/image markers at follow-up.

3.4 Association between vascular markers and lung deformation

Tab. 3 synthesizes the associations found between vascular markers and the percent lung basal deformation (LBD) on the follow-up database. Significant strong correlations were found between peripheral vascular indexes –PCI, PVD) and LBD at M3, and also between the peripheral vascular density follow-up PVD (M3 – M0) and LBD(M3). A moderate non-significant correlation was registered between BV5/BV50 and LBD at M3 but a strong significant correlation was noticed between the BV5/BV50 difference at inspiration versus expiration and LBD at M3. Figure 12 illustrates the significant correlations found in Tab. 3.

Tab. 3. Association between vascular markers and lung deformation (Pearson correlation coefficient).

Silicovilung	**PCI(M3)**	**PVD(M3)**	**PVD(M3) - PVD(M0)**	**BV5/BV50 inspi (M3)**	**BV5/BV50 difference (inspi-expi) at M3**
LBD(M3)	**0.707**	**0.708**	**0.66**	0.42	**0.6**
p-value	*0.01*	*0.01*	*0.02*	*0.07*	*0.007*

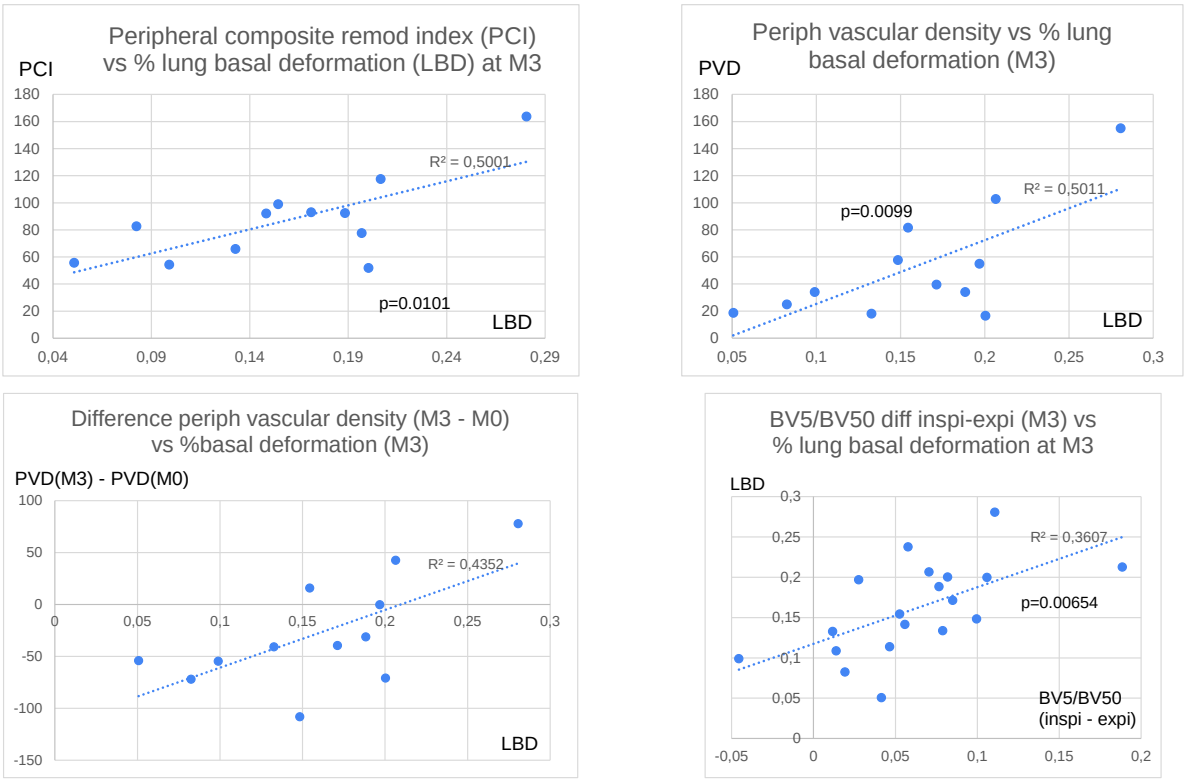

Fig. 12. Significant associations between vascular markers and lung deformation.

To resume, despite the limited available dataset at the time of the study, these findings emphasize the interest of the proposed CT vascular remodeling biomarkers in COVID-19 analysis and follow-up. They introduce quantitative measures based on standard CT imaging to either reinforce or complement additional clinical findings potentially requiring complex imaging or functional investigations. The different correlations found with functional, radiological and morphological parameters suggest the ability of vascular remodeling biomarkers to capture residual vascular alterations in post-acute sequelae of COVID-19 in relation with the persistence of ground glass opacity and/or development of radiologic patterns suggestive for fibrosis, such as reticulations.

We note the central position that peripheral vascular markers (PCI and PCV) occupy in correlations with other morphological and functional parameters, suggesting a potential key role in monitoring the sequelae of COVID-19.

4. Conclusion

This paper proposed a series of vascular remodeling biomarkers obtained from CT quantitative analysis, with a particular focus on the peripheral lung area, in order to investigate the possibility to capture residual vascular alteration in post-acute sequelae of COVID-19 (PASC). The significant moderate-to-strong correlations between vascular biomarkers on follow-up, and clinical and morphological parameters suggest a link between the persistence of vascular alterations in PASC and the development of fibrotic patterns, which is a promising direction for future research.

In conclusion, quantitative vascular remodeling biomarkers associating complementary analysis of lung structures

(parenchyma texture, and inspiration/expiration deformation patterns) can add to the knowledge on COVID-19 injury mechanisms and be a significant help in severity diagnosis and prediction of the evolution of this pathology.

Acknowledgement

The study was funded by the ANR SILICOVILUNG aapCOVID2020, France.

References

1. George PM, Wells AU, Jenkins RG, "Pulmonary fibrosis and COVID-19: the potential role for antifibrotic therapy", *Lancet Respir Med.*, 2020.
2. Synn AJ, Li W, Estépar RSJ, Washko GR, O'Connor GT, Tsao CW, Mittleman MA, Rice MB, "Pulmonary Vascular Pruning on Computed Tomography and Risk of Death in the Framingham Heart Study", AJRCCM, sept. 2020, 0.1164/rccm.202005-1671LE.
3. Lins et al., "Assessment of Small Pulmonary Blood Vessels in COVID-19 Patients Using HRCT", Academic Radiology, Vol 27, No 10, October 2020, https://doi.org/10.1016/j.acra.2020.07.019
4. A.F.Kouvahé, C.Fetita, "A Generic Approach for Efficient Detection of Vascular Structures", IRBM 2020, https://doi.org/10.1016/j.irbm.2020.06.011
5. Fetita et al, "A morphological-aggregative approach for 3D segmentation of pulmonary airways from generic MSCT acquisitions", The second International Workshop on Pulmonary Analysis, MICCAI 2009, p. 215-226.
6. Fetita et al., "Robust lung identification in MSCT via controlled flooding and shape constraints: dealing with anatomical and pathological specificity," in SPIE Medical Imaging 2016: Biomedical Applications in Molecular, Structural, and Functional Imaging vol. 9788, 2016.
7. Fetita C., *et al*, "Airway shape assessment with visual feed-back in asthma and obstructive diseases", in Medical Imaging 2010: Visualization, Image-Guided Procedures, and Modeling, Proceedings of SPIE Vol. 7625, p. 76251E:1-12.
8. Fetita et al., "Diffusion-based interpolation with geometrical constraints applied to investigation of interstitial lung diseases", IEEE-BIBE 2020.